Gas sensor array assisted with UV illumination for discriminating several analytes at room temperature

Mohsen Naeimi Pour[1], *Alireza Nikfarjam*[2], *Asghar Taheri*[1] ✉, *Ahmad Reza Sadredini*[2]

[1]*Department of Electrical Engineering, Faculty of Engineering, University of Zanjan, University St. IR-313-45195, Zanjan, Iran*
[2]*Faculty of New Sciences & Technologies, University of Tehran, P.O. Box 14395-1561, Tehran, Iran*
✉ *E-mail: taheri@znu.ac.ir*

Published in Micro & Nano Letters; Received on 20th January 2019; Revised on 19th April 2019; Accepted on 23rd May 2019

In this work, a metal-oxide gas sensor array was fabricated for discriminating several gases at room temperature using ultraviolet (UV) illumination. The sensor array consisted of four interdigitated gold microelectrodes, and titanium dioxide (TiO_2) nanofibres were electrospun on them. The nanofibres were calcined at 550°C for 1 h. Finally, one of these sensors was coated with a thin layer of gold (Au) using DC sputtering method at a thickness of 2 nm. Similarly, the other two sensors were coated with a thin layer of platinum (Pt) and copper (Cu), respectively, and the last one remained uncoated. The nanofibres were characterised by scanning electron microscope, X-ray diffraction, and UV spectroscopy. The examined analytes were methanol, ethanol, NH_3, and acetone, each at seven various concentration levels, including 50, 100, 150, 200, 300, 400, and 500 ppm. Principal component analysis and linear discriminant analysis were used to evaluate the proposed technique. The results demonstrated that the sensor array along with UV illumination could successfully discriminate the analytes at room temperature.

1. Introduction: Nowadays, gas sensors play a significant role in different applications, and various sensing technologies have been developed for gas identification [1–3]. Among them, metal-oxide gas sensors have attracted much attention due to excellent properties including small size, low cost, high sensitivity, short response time, easy manufacturing, and so on [4–8]. Despite these positive features, metal-oxide gas sensors suffer from the drawbacks of poor selectivity, which greatly limit their industrial and commercial applications [9, 10]. Hence, these sensors fall short when they are utilised to discriminate between various analytes. Several techniques have been proposed to overcome the problem [11–16]. One of the most important approaches for improving selectivity is using sensor arrays, which are composed of different sensing elements to detect the analyte with data of higher dimensions [14, 17]. In other words, sensor arrays can identify analytes based on fingerprints obtained from gas sensors.

Operating at high temperatures is another disadvantage of these sensors [16, 18–21]. Metal-oxide gas sensors usually operate at elevated temperatures, which lead to high power consumption and lifetime degradation. Different techniques for solving the problem of high operating temperature have been reported in the previous studies such as doping with noble metals, surface decoration with various catalyst materials, ultraviolet (UV) light stimulation and so on [22–25]. Among them, UV light stimulation in photocatalytic metal oxides has attracted much interest to activate the chemical reactions at low operating temperatures in related sensors [22, 23].

Up to now, different nanostructures of the metal-oxide gas sensors have been developed in previous studies such as nanofibres, nanowires, nanotubes, and nanosheets [26–28]. Due to the high surface-to-volume ratio in nanostructure metal-oxide semiconductors, such as nanofibres, they are good candidates for gas sensing applications.

To the best of our knowledge, there is no study on using metal-oxide gas sensor arrays along with UV illumination for the discrimination of various gases at room temperature. Thus, it is worthy of paying attention to this technique. In this Letter, a gas sensor array based on titanium dioxide (TiO_2) nanofibres was fabricated, and the sensor array along with UV illumination was successfully utilised to discriminate several analytes at room temperature. For evaluating the validity of the proposed method, four different analytes including methanol, ethanol, acetone, and ammonia (NH_3) were introduced as target gases.

2. Materials and methods

2.1. Sensor array fabrication: The sensor array was composed of four interdigitated gold microelectrodes which were fabricated by DC sputtering, photolithography, and wet etching techniques. Each sensor consisted of 40 electrode finger pairs with 2.8 mm length, 40 μm interval, and 30 μm width.

TiO_2 nanofibres were synthesised by electrospinning technique. A typical experimental method to prepare the electrospinning solution is as follows [29]: precursor solution was prepared by dissolving polyvinyl pyrrolidone (PVP) (12 wt%) in 2.75 ml ethanol. In another container, 0.4 g titanium tetraisopropoxide [Ti(OiPr)4; 97%, Sigma-Aldrich] was mixed with 1 ml ethanol and 1 ml acetic acid for 30 min and then added to the first solution. This mixture was stirred for 2 h at 65°C to obtain a homogeneous viscous solution. The obtained solution loaded into a plastic syringe equipped with a stainless steel needle and a voltage of 11 kV was applied between the needle of the syringe and the collector plate over a separation distance of 10 cm. The feeding rate was kept constant at 1 ml/h. The obtained solution was electrospun on the gold interdigitated microelectrodes and annealed for 20 min at 120°C for removing the volatile impurities. The resultant nanofibres were calcined at 550°C for 1 h to obtain TiO_2 nanofibres. Finally, one of these sensors was coated with a thin layer of gold (Au) using DC sputtering method at a thickness of 2 nm. Similarly, the other two sensors were coated with a thin layer of platinum (Pt) and copper (Cu), respectively, and the last one remained uncoated.

2.2. Characterisation: The TiO_2 nanofibres were studied by a scanning electron microscope (SEM, XL 30, Philips, USA). X-ray diffraction (XRD) analysis was carried out by a Philips X'Pert MPD instrument operating with CuKα radiation ($\lambda = 1.54178$ A) at a voltage of 40 kV and current of 30 mA.

doi: 10.1049/mnl.2019.0049

An Evolution 300 spectrophotometer (UV-1700 Shimadzu) was used to record the UV–vis absorption spectra.

2.3. Experimental details: The experimental setup used for recording the responses of the sensor array is schematically presented in Fig. 1. The experiments were carried out in a glass chamber of 10 l volume. The examined analytes were methanol, ethanol, NH_3, and acetone, each at seven various concentration levels, including 50, 100, 150, 200, 300, 400 and 500 ppm. In each experiment, a predetermined amount of the analyte was injected into the gas chamber and was evaporated in the chamber using a heater. The atmosphere of the chamber was homogenised by an electric fan placed inside the chamber.

In each experiment to insert the sensor array into the gas chamber, the chamber lid was opened, and the sensor array was placed with a distance of 3 cm from the UV-LED. The measured power of the UV-LED at this distance was about 600 μW/cm^2. Each sensor was connected in series to a 56 kΩ resistor (R_1) and a voltage source (10 Vdc). For each sensor, the electric circuit converts the variation of the sensor resistance (R_s) into a voltage signal, which is approximately proportional to the conductance of the gas sensor $(R_1 \ll R_s)$.

3. Results and discussion

3.1. Structural analysis: The morphology of electrospun nanofibres was characterised by SEM images. Fig. 2 represents the SEM images of TiO_2 nanofibres before and after calcination. As shown, the morphology of the nanofibres was completely smooth and uniform before calcination (Fig. 2*a*). Even though calcination influenced on the average diameter of the nanofibres and decreased the mean value of the diameters from ~850 to ~270 nm, their morphology remained as continuous structures (Fig. 2*b*).

The crystal structure and phase evolution of the calcinated TiO_2 nanofibres were determined by XRD technique. The XRD patterns indicated that calcinated TiO_2 nanofibres consisted of both anatase and rutile phases (Fig. 3). As shown, the peaks at 25°, 48°, and 55° were related to anatase phase while the peaks at 27° and 36° were related to the rutile phase of TiO_2 nanofibres. Calcination temperature of TiO_2 nanofibres plays a crucial role in their photocatalytic activity. Although the anatase phase is one of the best photocatalysts, the rutile phase has more stability [23]. Moreover, the anatase phase has a higher bandgap than the rutile phase.

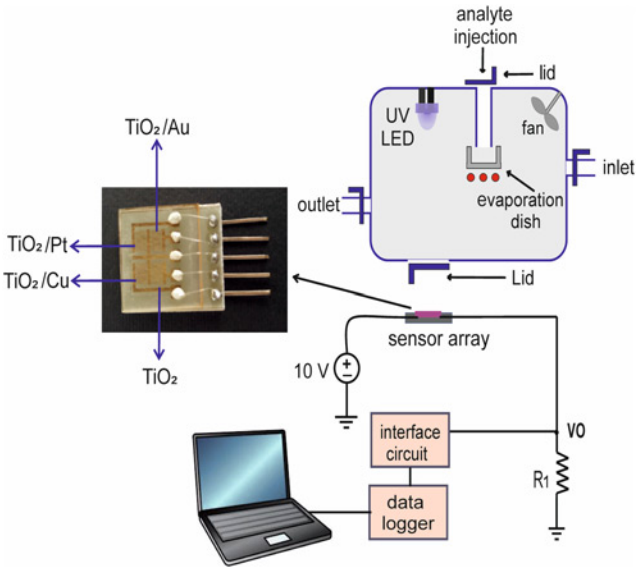

Fig. 1 *Schematic diagram of the experimental setup*

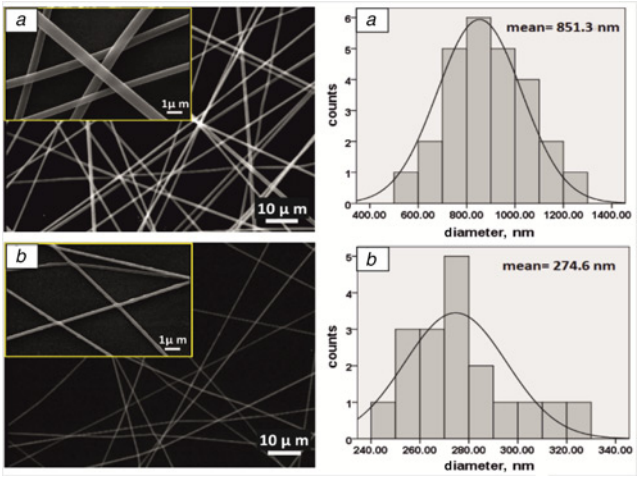

Fig. 2 *SEM images and diameter distribution histograms of TiO_2 nanofibres*
a Before calcination
b After calcination

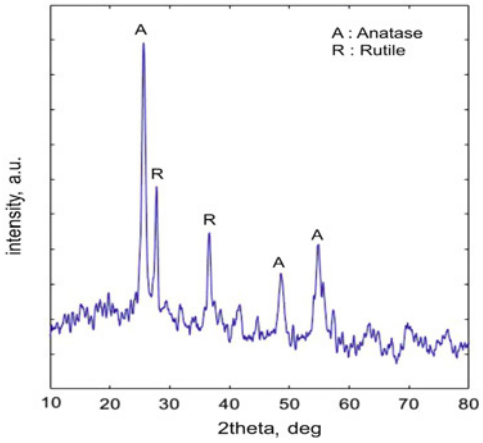

Fig. 3 *XRD pattern of the TiO_2 nanofibres calcined at 550°C*

Thus the increasing rutile phase leads to shifting maximum absorption spectra to a larger wavelength [23].

The absorption spectrum of the TiO_2 nanofibres revealed that the maximum absorption wavelength was located at 369 nm (Fig. 4). Thus, in this Letter, a 365 nm UV-LED was chosen for maximum absorption.

3.2. Experimental gas sensing results: In each experiment, the sensor array was exposed to the analyte under UV irradiation until the responses reach the steady-state and finally, UV-off and the sensor array was removed from the chamber. According to Fig. 1, the sensor response is defined as $(Vo_2–Vo_1)/Vo_1$, where Vo_1 is the output voltage in clean air and Vo_2 is the output voltage when sensor responses to the test gas under UV illumination. Figs. 5*a–d* depict the response of the TiO_2/Au sensor under UV illumination conditions in 100 ppm for several gases. As shown, the highest response belongs to ethanol; thus Au is a good catalyst for the detection of ethanol in comparison with other gases.

The response of sensors under UV illumination conditions in 100 ppm methanol is shown in Figs. 6*a–d*. Among four sensors, TiO_2/Au sensor displayed higher sensitivity to methanol than the rest (34%). Also, the response times of these sensors to 100 ppm of methanol were 71, 73, 77, and 81 s for TiO_2/Au, TiO_2/Pt, TiO_2/Cu, and TiO_2, respectively.

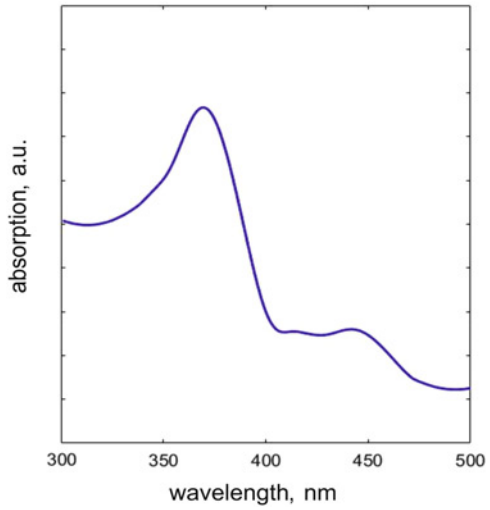

Fig. 4 *Absorption spectrum of TiO_2 nanofibres*

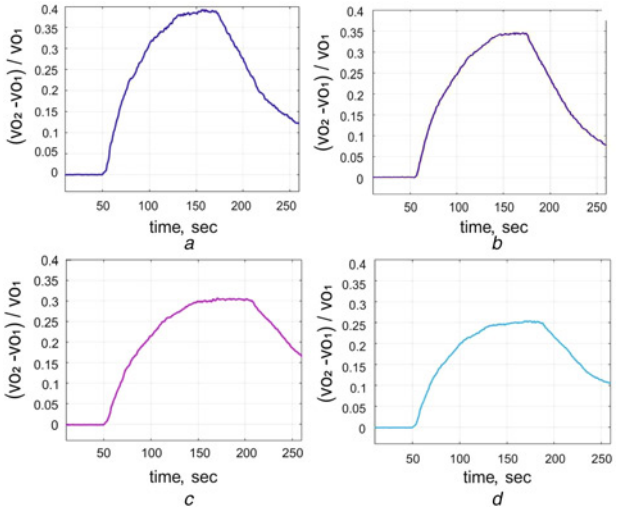

Fig. 5 *Response of the TiO_2/Au sensor under UV illumination conditions in the presence of 100 ppm for several gases*
a Ethanol
b Methanol
c NH_3
d Acetone

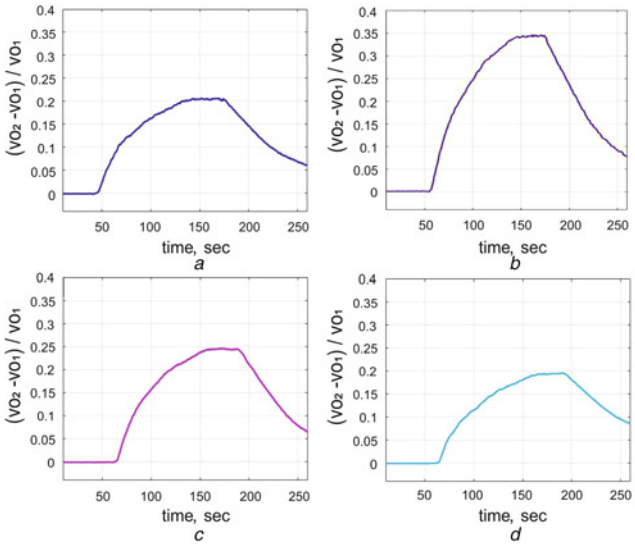

Fig. 6 *Response of sensors under UV illumination conditions in 100 ppm methanol*
a TiO_2/Cu
b TiO_2/Au
c TiO_2/Pt
d TiO_2

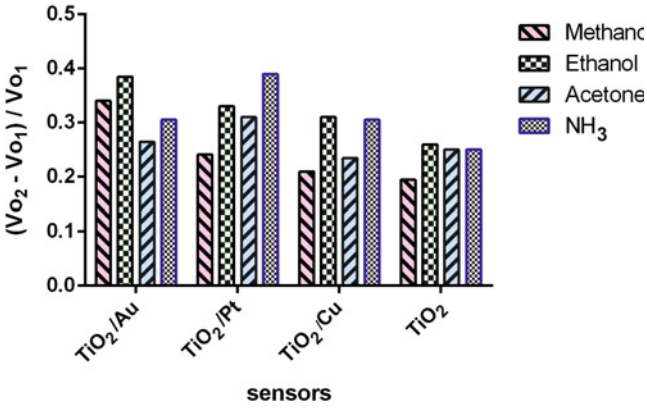

Fig. 7 *Response of the sensor array under UV light illumination conditions in 100 ppm for various analytes*

As shown in Fig. 7 when the sensor array is exposed to an analyte under UV illumination, each sensing element responses uniquely. The combination of the sensors response can be considered as the analyte 'fingerprint'. It is important to note that there was no response to the gases at temperatures below 200°C without UV illumination.

The sensor responses were assumed as the features of the analyte. The four sensors and the four different analytes, each at seven various concentrations produced a total of 28×4 feature vectors as the dataset. Principal component analysis (PCA) and linear discriminant analysis (LDA) were used to evaluate the proposed technique. PCA is a useful mathematical algorithm for dimensionality reduction [30] and does not utilise the category information. Fig. 8 shows the result of the PCA mapping of the feature vectors to a three-dimensional (3D) feature space. As shown, except acetone and ethanol clusters which were close together, clusters of other gases were obviously discriminated.

LDA is another statistical method for dimensionality reduction [31] and is based on the maximisation of the variance between

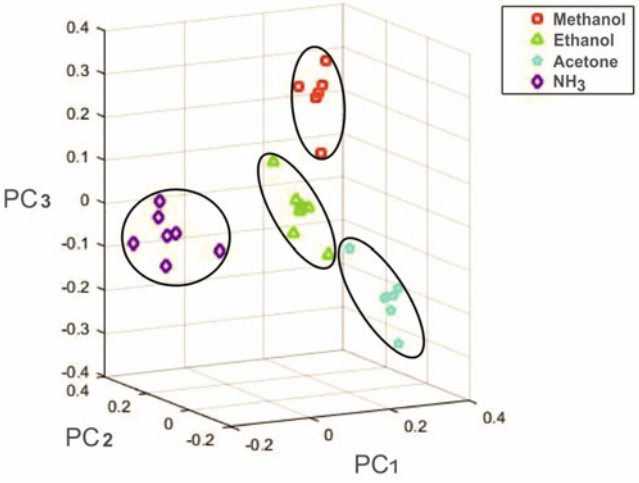

Fig. 8 *Result of PCA mapping of the feature vectors of the four analytes, each at different concentrations, to a 3D feature space*

doi: 10.1049/mnl.2019.0049

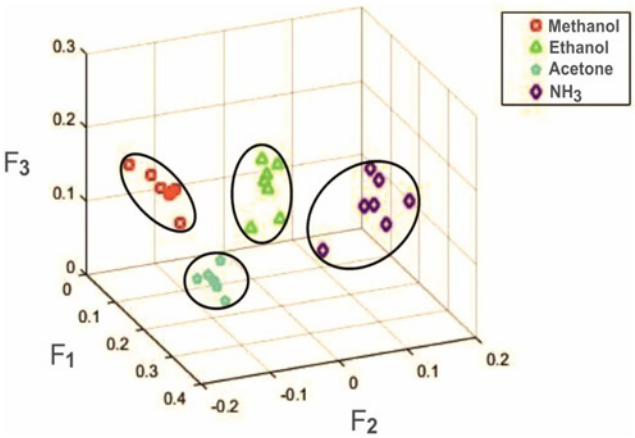

Fig. 9 *Classification of four various analytes, each at different concentrations, using a 3D LDA feature space*

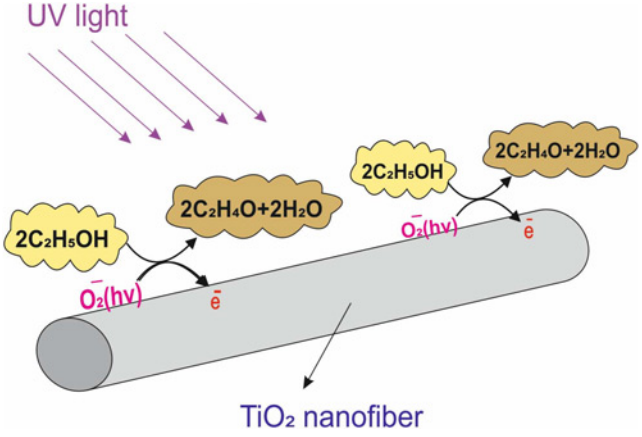

Fig. 10 *Schematic diagram of the UV-activated room temperature gas sensing mechanism*

classes and minimisation of the variance within classes to optimise the discrimination between classes [32]. Unlike PCA, the LDA method requires category information. LDA applied on the sensor array dataset is shown in Fig. 9. The result indicated 100% success in the classification of studied gases at room temperature. Compared to PCA results, the LDA presented more discrimination and decreased overlapping between classes and thus showed better performance. In previously studied metal-oxide based sensor arrays, the operating temperature range for detecting various gases was between 150 up to 500°C [15, 33–35], while the proposed technique enables the sensor array to discriminate several analytes at room temperature. Other photocatalyst metal-oxide gas sensors are also expected to fit the proposed technique. In this Letter, all examined gases were successfully discriminated at room temperature. Thus, the proposed technique opens up a promising way for identifying the gas species in many industrial and domestic applications, especially in an explosive and flammable gas atmosphere. On the other hand, low power consumption is a basic requirement for gas sensors in many fields, such as wireless applications. An example of using gas sensors in wireless applications is ingestible capsules, which are a powerful tool for monitoring human health, and they can identify different gases in the gut [36, 37]. Moreover, the proposed technique can be used in smart nanosensor systems which implement as a safety feature in mobile phones and smartwatches [38].

4. Gas-sensing mechanism: The sensing mechanism of the UV-activated gas sensor can be described as follows: In dark condition, oxygen molecules in the atmosphere receive free electrons from TiO_2 and oxygen ions (O_2^-) are formed on the surface of TiO_2 nanofibres. When the sensor is stimulated by UV illumination that has higher energy than the bandgap of the TiO_2, electron–hole pairs are generated [39] and the photo-induced holes react with the adsorbed oxygen ions, which lead to the removal of the oxygen molecules from the surface of TiO_2 nanofibres according to the following reactions [40]:

$$h\nu \rightarrow e^- + h^+ \quad (1)$$

$$h^+ + O_2^- \rightarrow O_{2(gas)} \quad (2)$$

Meanwhile, oxygen molecules in the atmosphere react with the photo-induced electrons, and photo-induced oxygen ions $O_2^-(h\nu)$ are created on the surface of the sensor [40]

$$O_2 + e^-(h\nu) \rightarrow O_2^-(h\nu) \quad (3)$$

Unlike oxygen ions that are thermally stable and difficult to be removed from the surface of TiO_2 at room temperature, the photo-induced oxygen ions are weakly bonded to TiO_2 and can be easily removed at room temperature [40]. As a result, the photo-induced oxygen ions play a very important role in the UV-activated gas sensing mechanism Fig. 10. When the reducing agents were introduced to the sensor surface, the reducing agents react with the photo-induced oxygen ions, and the electrons are released from this reaction, which leads to an increase in conductance [40]. For example, the reaction between ethanol molecules and the photo-induced oxygen ions is as follows:

$$2C_2H_5OH + O_2^-(h\nu) \rightarrow 2C_2H_4O + 2H_2O + e^- \quad (4)$$

As a result, in the photocatalytic metal-oxide gas sensor, UV illumination can activate the chemical reactions at low operating temperatures.

5. Conclusion: A gas sensor array assisted with UV illumination was introduced for discriminating several analytes at room temperature. The analytes examined were methanol, ethanol, acetone, and NH_3 at the concentration levels ranging from 50 to 500 ppm. PCA and LDA were utilised to evaluate the proposed technique. PCA results showed somehow overlapping between acetone and ethanol clusters, while other gases were segregated in the feature space. LDA results provided better performance, and all target gases were vividly discriminated in the feature space. The results demonstrated that the proposed technique could successfully meet the needs in the mentioned conditions. By integrating the sensor array with the supporting electronic circuitry, it can be used as a portable and cost-effective gas analyser.

6 References

[1] Algadri N.A., Hassan Z., Ibrahim K., *ET AL.*: 'A high-sensitivity hydrogen gas sensor based on carbon nanotubes fabricated on glass substrate', *J. Electron. Mater.*, 2018, **47**, (11), pp. 6671–6680
[2] Liang S., Li J., Wang F., *ET AL.*: 'Highly sensitive acetone gas sensor based on ultrafine α-Fe_2O_3 nanoparticles', *Sens. Actuators, B, Chem.*, 2017, **238**, pp. 923–927
[3] Tabassum S., Kumar R., Dong L.: 'Plasmonic crystal-based gas sensor toward an optical nose design', *IEEE Sens. J.*, 2017, **17**, (19), pp. 6210–6223
[4] Kwon Y.J., Na H.G., Kang S.Y., *ET AL.*: 'Attachment of Co_3O_4 layer to SnO_2 nanowires for enhanced gas sensing properties', *Sens. Actuators B, Chem.*, 2017, **239**, pp. 180–192
[5] Nikfarjam A., Fardindoost S.: 'Fabrication of Pd doped WO_3 nanofiber as hydrogen sensor', *Polymers*, 2013, **5**, (1), pp. 45–55

[6] Nikfarjam A., Hosseini S., Salehifar N.: 'Fabrication of a highly sensitive single aligned TiO_2 and gold nanoparticle embedded TiO_2 nano-fiber gas sensor', *ACS Appl. Mater. Interfaces*, 2017, **9**, (18), pp. 15662–15671

[7] Vallejos S., Grácia I., Chmela O., *et al.*: 'Chemoresistive micromachined gas sensors based on functionalized metal oxide nanowires: performance and reliability', *Sens. Actuators B, Chem.*, 2016, **235**, pp. 525–534

[8] Wang Y., Liu J., Cui X., *et al.*: 'NH_3 gas sensing performance enhanced by Pt-loaded on mesoporous WO_3', *Sens. Actuators B, Chem.*, 2017, **238**, pp. 473–481

[9] Barsan N., Koziej D., Weimar U.: 'Metal oxide-based gas sensor research: how to?', *Sens. Actuators B, Chem.*, 2007, **121**, (1), pp. 18–35

[10] Zhang G., Han X., Bian W., *et al.*: 'Facile synthesis and high formaldehyde-sensing performance of NiO–SnO_2 hybrid nanospheres', *RSC Adv.*, 2016, **6**, (5), pp. 3919–3926

[11] Herrero-Carrón F., Yánez D.J., de Borja Rodríguez F., *et al.*: 'An active, inverse temperature modulation strategy for single sensor odorant classification', *Sens. Actuators B, Chem.*, 2015, **206**, pp. 555–563

[12] Hossein-Babaei F., Amini A.: 'A breakthrough in gas diagnosis with a temperature-modulated generic metal oxide gas sensor', *Sens. Actuators B, Chem.*, 2012, **166**, pp. 419–425

[13] Leidinger M., Sauerwald T., Conrad T., *et al.*: 'Selective detection of hazardous indoor VOCs using metal oxide gas sensors', *Procedia Eng.*, 2014, **87**, pp. 1449–1452

[14] Ng K.T., Boussaid F., Bermak A.: 'A CMOS single-chip gas recognition circuit for metal oxide gas sensor arrays', *IEEE Trans. Circuits Syst. I, Regul. Pap.*, 2011, **58**, (7), pp. 1569–1580

[15] Yang W., Wan P., Jia M., *et al.*: 'A novel electronic nose based on porous In_2O_3 microtubes sensor array for the discrimination of VOCs', *Biosens. Bioelectron.*, 2015, **64**, pp. 547–553

[16] Yin X., Zhang L., Tian F., *et al.*: 'Temperature modulated gas sensing E-nose system for low-cost and fast detection', *IEEE Sens. J.*, 2016, **16**, (2), pp. 464–474

[17] Yi S., Tian S., Zeng D., *et al.*: 'A novel approach to fabricate metal oxide nanowire-like networks based coplanar gas sensors array for enhanced selectivity', *Sens. Actuators B, Chem.*, 2014, **204**, pp. 351–359

[18] Song N., Jiang H., Cui T., *et al.*: 'Synthesis and enhanced gas-sensing properties of mesoporous hierarchical α-Fe_2O_3 architectures from an eggshell membrane', *IET Micro Nano Lett.*, 2012, **7**, (9), pp. 943–946

[19] Sun X., Liu X., Deng X., *et al.*: 'Synthesis of Zn-doped In_2O_3 nano sphere architectures as a triethylamine gas sensor and photocatalytic properties', *RSC Adv.*, 2016, **6**, (92), pp. 89847–89854

[20] Tyagi P., Sharma A., Tomar M., *et al.*: 'Metal oxide catalyst assisted SnO_2 thin film based SO_2 gas sensor', *Sens. Actuators B, Chem.*, 2016, **224**, pp. 282–289

[21] Wang X., Zhao M., Liu F., *et al.*: 'C_2H_2 gas sensor based on Ni-doped ZnO electrospun nanofibers', *Ceram. Int.*, 2013, **39**, (3), pp. 2883–2887

[22] Meng F., Zheng H., Sun Y., *et al.*: 'UV-activated room temperature single-sheet ZnO gas sensor', *Micro Nano Lett.*, 2017, **12**, (10), pp. 813–817

[23] Nikfarjam A., Salehifar N.: 'Improvement in gas-sensing properties of TiO2 nanofiber sensor by UV irradiation', *Sens. Actuators B, Chem.*, 2015, **211**, pp. 146–156

[24] Sakthivel B., Manjakkal L., Nammalvar G.: 'High performance CuO nanorectangles-based room temperature flexible NH_3 sensor', *IEEE Sens. J.*, 2017, **17**, (20), pp. 6529–6536

[25] Wang L., Wang Y., Yu K., *et al.*: 'A novel low temperature gas sensor based on Pt-decorated hierarchical 3D SnO_2 nanocomposites', *Sens. Actuators B, Chem.*, 2016, **232**, pp. 91–101

[26] Arnold M.S., Avouris P., Pan Z.W., *et al.*: 'Field-effect transistors based on single semiconducting oxide nanobelts', *J. Phys. Chem. B*, 2003, **107**, (3), pp. 659–663

[27] Han J.-W., Rim T., Baek C.-K., *et al.*: 'Chemical gated field effect transistor by hybrid integration of one-dimensional silicon nanowire and two-dimensional tin oxide thin film for low power gas sensor', *ACS Appl. Mater. Interfaces*, 2015, **7**, (38), pp. 21263–21269

[28] Li T., Zeng W., Long H., *et al.*: 'Nanosheet-assembled hierarchical SnO_2 nanostructures for efficient gas-sensing applications', *Sens. Actuators B, Chem.*, 2016, **231**, pp. 120–128

[29] Kumar A., Jose R., Fujihara K., *et al.*: 'Structural and optical properties of electrospun TiO_2 nanofibers', *Chem. Mater.*, 2007, **19**, (26), pp. 6536–6542

[30] Akbar M.A., Ali A.A.S., Amira A., *et al.*: 'An empirical study for PCA-and LDA-based feature reduction for gas identification', *IEEE Sens. J.*, 2016, **16**, (14), pp. 5734–5746

[31] Amini A., Hosseini-Golgoo S.M.: 'Rapid recognition of airborne combustible molecules with an operating temperature-modulated gas sensor', *Sens. Lett.*, 2012, **10**, (3–4), pp. 821–825

[32] Zhang H., Wang J.: 'Detection of age and insect damage incurred by wheat, with an electronic nose', *J. Stored Prod. Res.*, 2007, **43**, (4), pp. 489–495

[33] Horsfall L.A., Pugh D.C., Blackman C.S., *et al.*: 'An array of WO_3 and CTO heterojunction semiconducting metal oxide gas sensors used as a tool for explosive detection', *J. Mater. Chem. A*, 2017, **5**, (5), pp. 2172–2179

[34] Li X., Cho J.H., Kurup P., *et al.*: 'Novel sensor array based on doped tin oxide nanowires for organic vapor detection', *Sens. Actuators B, Chem.*, 2012, **162**, (1), pp. 251–258

[35] Prajapati C.S., Soman R., Rudraswamy S., *et al.*: 'Single chip gas sensor array for air quality monitoring', *J. Microelectromech. Syst.*, 2017, **26**, (2), pp. 433–439

[36] Bettinger C.J.: 'Advances in materials and structures for ingestible electromechanical medical devices', *Angew. Chem. Int. Ed.*, 2018, **57**, (52), pp. 16946–16958

[37] Kalantar-Zadeh K., Berean K.J., Ha N., *et al.*: 'A human pilot trial of ingestible electronic capsules capable of sensing different gases in the gut', *Nat. Electron.*, 2018, **1**, (1), p. 79

[38] Aoki P.M., Honicky R., Mainwaring A., *et al.*: 'Common sense: Mobile environmental sensing platforms to support community action and citizen science'. Adjunct Proc. of the Tenth Int. Conf. on Ubiquitous Computing, Seoul, Republic of Korea, 2008

[39] Lin C.-h., Chang S.-J., Chen W.-S., *et al.*: 'Transparent ZnO-nanowire-based device for UV light detection and ethanol gas sensing on c-Si solar cell', *RSC Adv.*, 2016, **6**, (14), pp. 11146–11150

[40] Fan S.-W., Srivastava A.K., Dravid V.P.: 'UV-activated room-temperature gas sensing mechanism of polycrystalline ZnO', *Appl. Phys. Lett.*, 2009, **95**, (14), p. 142106

doi: 10.1049/mnl.2019.0049